The Thermal Transfers of a Habitable Envelope in an Extremely Dry Area and These Effects on Thermal Comfort

Oudrane A[1,2]*, Hamouda M* [2], Aour B [3]

[1]Faculty of Science and Technology, University El-Wancharissi of Tissemsilt (CUT), Road Bougra Ben Hamouda, 38004, Tissemsilt, (Algeria).

[2]Laboratoire de developpement durable et informatique, Université Ahmed Draia, Adrar, (Algeria).

[3]Laboratory of Applied Biomechanics and Biomaterials (LABAB), Polytechnic School of Oran-Maurice Audin (ENPO-MA), BP 1523 El Mnaour, 31000, Oran, (Algeria).

[*]Corresponding author; Email: abdellatif.habadat@gmail.com.

Article Info

ABSTRACT

The main goal in this work is the thermal modeling of occupant comfort in new habitable architectures for a dry climate in the region of Adrar in Algeria. This thermal modeling aims to determine the parameters that affect the thermal comfort of the occupants in this climate. To achieve this goal, mathematical models describing thermal exchanges in an individual habitat have been developed. These models are established on the basis of the thermal balance at the level of each wall in habitat. The results obtained were calibrated using climatic data recently measured by the renewable energy research unit of the Saharan medium in Adrar. A detailed analysis of certain parameters influencing thermal comfort in this habitat was mentioned and discussed. The fundamental equations governing thermal exchanges have been concretized by an implicit method of finite differences, based on the nodal procedure. The system of algebraic equations obtained was solved by the iterative Gaussian method. The results of the numerical simulation have shown that the material currently used in the construction of this habitat, as well as the current climatic conditions, are the fundamental causes of undesirable overheating in this dry region.

Nomenclature

e	The material thickness	m	PE	East wall
hc	Coefficient of internal heat exchange by convection	$W.m^{-2}.k^{-1}$	PN	North wall
m_{ps}	The south wall Mass	Kg	PO	West wall
P_{absor}	Amount of heat absorbed	W	PS	South wall
S_{PL}	South wall surface	m^2	PFP	The ceiling Wall
T_{amb}	Ambient temperature	$°C$	PNI	Internal north wall
T_{soil}	Soil temperature	$°C$	PSI	Internal south wall
T_{air}	Air temperature	$°C$	PFPI	Internal wall of the ceiling
ΔT	Temperature difference	$°C$	PSE	External south wall
T_{int}	Full air temperature in the habitat	$°C$	POE	External west wall
T_{ext}	Outside air temperature	$°C$	PIP	Internal floor wall
T_b	Temperature of the concrete slab	$°C$	PEE	Externe east wall
T_C	Thermal comfort temperature	$°C$	PFPE	External wall of the ceiling
FSG	Global solar flux	W/m^2	M'zab	Region north of Sahara Algerian

I.   Introduction

The whole world has been facing an increase in energy consumption in a way that has been increasing for decades. This increase fundamentally calls into question the economic model which is tributary for its development on a colossal quantity of energy [1]. The energy performance of a habitat can be estimated by performing thermodynamic simulations that take into account different conventional assumptions such as: the weather, occupancy, temperature set points, and uses of the window and shutter by the occupants and even the architecture of the habitats. The experience feedbacks in the habitable envelope with high energy performance highlight significant differences in energy consumption between forecasts and summer overheating [2]. The development of a good energy concept for a house involves the search for a balance between reinforced insulation, compactness, passive solar gains, thermal inertia and comfort, indoor air quality and investment cost. This has been the subject of specific attention since the pre-project phase and most often requires the use of premature studies [3]. The essential function of a house is to ensure an interior ambiance well suited to our needs and our comfort. The inhabitant often places his comfort before saving energy. It is therefore necessary to plan the construction and installations to consume less energy while ensuring adequate comfort [4].

Saheli and al [5] studied the influence of climatic conditions on the local heating efficiency of a building installed in the South Algeria. Furthermore, Benhammou and al [6, 7] analyzed the thermal behavior of a housing submitted to periodic solicitations under hot and dry climate. This analysis was made for the hottest July in the summer season, in order to examine the effect combined of the heat insulation and the passive cooling by EAHE on the thermal performances of the habitable envelopes for desert regions in the South Algeria.

This numerical study consists of visualizing not only the impact of climatic conditions and building materials used in Adrar region's architecture on thermal comfort, but also its effects on the main heat transfer mechanisms related to the thermal comfort process. In addition, from the results of numerical investigation of different variables such as: internal temperature, external temperature and the density of the solar flux, we show ourselves such an approach which allows improving the thermal comfort in this architecture.

II.   Domestic architecture

The raw earth is a material available everywhere in the planet. It is the universal material the privileged and the easiest handled by the human being to make a shelter while several millennia. Globally, earthen houses today house more than a third of the world's population [8]. This construction material, respects the man and the environment, is perfectly recyclable. It ensures thermal comfort by its characteristics and offers advantageous economic convenience.

Algeria, this vast territory has experienced diversified land architecture according to the diversity of climatic zones. The domestic conception of Adrar region, south-west of the Sahara, differs from that of Algiers, or that of M'zab valley at Ghardaïa, at the lower Sahara. The model of earth allows a real diversity of architectural language [8]. Unfortunately, since the floods of 2009 (see Figure 1), the use of this material is banned, and replaced by cement (reinforced concrete).

Figure 1. Damage to equipment due to floods in Adrar region.

This material seen as modernity symbol and social promotion. In Figure 2, we present the new architecture of Adrar region which is based on reinforced concrete without total control of thermal insulation.

Figure 2. New reinforced concrete architecture in Adrar region.

On the other hand, in Figure 3 we present the old architecture of this region. This architecture allows a thermal insulation based on the raw earth. The latter played the role of an insulating material against thermal discomfort.

Figure 3. The old architecture with raw earth in Adrar region.

III.   Climatological Characteristics

The Adrar has a typical hot desert climate of the hyper-dry Saharan zone. It's the heart of Sahara, with a hot, very long summer and a hot short, moderate winter. The annual average of precipitation in this region reaches hardly 14-15 mm, falling essentially in autumn or to spring [9].

The maximal average temperatures are 46 - 48 °C in July (the hottest month), what makes of Adrar one of the world hottest cities. As an example: the peak of record temperature was established on Monday, July 9th, 2018 with a temperature of 65 °C [10,11,12].

III.1. Solar data of the typical day chosen in adrar region

The table 1 presents the technical report of the solar data for the typical day of year 2014. This report is obtained by the radiometric station of the measures. Noting that these data will be used to calculate the different densities of solar flux influencing heat exchange in habitable envelope. These data were recently measured by a radiometric station to in the renewable energy research unit in the Saharan medium of Adrar ''URER'MS''.

This autonomous radiometric measuring station was realized at the end of 2010. Furthermore, it measures the global radiation parameters on three plans (Horizontal, Inclined at the latitude of the place and optimal monthly) and the ambient temperature. Figure 4 present a local image of this radiometric station in Adrar site.

Figure 4. Local picture of Adrar radiometric station.

Table 1. Technical report of the solar data for the typical day [11].

enerMENA High Precision Meteorological Station in Adrar, Algeria - 1 min												
Latitude: 27,88 °N				Altitude (amsl): 262 m								
Longitude: -0,27 °E				Station: CSPS.MT.09.203								
Time zone: 1 (UTC+1h)												

Date: jeudi, juil 17 2014 — DLR — day 198 year 2014 — CSP Services

Measured values:

GHI, DHI	Global Horizontal Irradiance in W/m², Diffus Horizontal Irradiance in W/m², each measured with a K&Z CMP21 pyranometer
DNI	Direct Normal Irradiance in W/m² measured with K&Z CHP1 pyrheliometer
T_{amb}, RH	Ambient Temperature in °C, Relative humidity in %, both measured with a Campbell CS215 Temperature and Humidity probe
WS, WS_{gust}	Wind speed in m/s, measured with NRG 40H Anemometer, WS_{gust}: maximal measured wind speed within the time interval
WD, WD_{StDev}	Wind direction in °N (to East), measured with NRG 200 Wind Direction Sensor. Standard deviation of wind direction within measurement interval.
BP	Air pressure from Campbell CS100 barometric pressure sensor
Acc.	Accuracy: deviation between measured and calculated DNI value from data base: $DNI_{measured}$ - $DNI_{calculated}$
Error	Error message recorded by the data logger. Full operation of the equipment is marked with a "0".
Cleaning	Cleaning of sensors: A cleaning event is marked with a "1".

Measured 1 min values													
value	GHI	DNI	DHI	T_{amb}	RH	WS	WS_{gust}	WD	WD_{StDev}	BP	Acc.	Error	Cleaning
unit	W/m²	W/m²	W/m²	°C	%	m/s	m/s	°N	°N	hPa	W/m²	#	#
min	0	0	0	32,5	4,5	0,0	0,0	0	0,0	980	-100,0		
max	1051	780	857	47,8	15,3	9,6	13,0	221	60,5	983	28,3	110000	1
average	323	231	136	40,7	9,9	4,1	5,8	110	17,5	981	-6,6		

The hourly distribution of the wind speeds represents an indicator for the wind potential. His knowledge allows the estimation of the wind energy available on the site. The Figure 5 represents the frequency distribution of average speeds measured for day given in percentage term for Adrar site.

The analysis of these curves shows that site of Adrar has important wind energy potential and which is more favorable to exploitation of this energy type for electricity production. The reached average speed is from 5 to 6m/s in July.
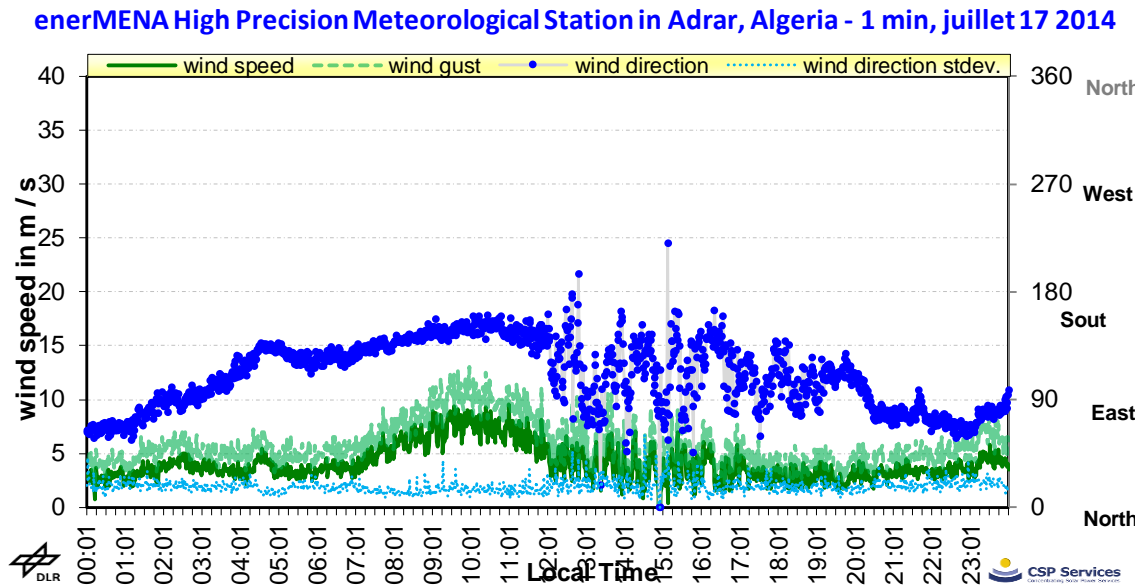
enerMENA High Precision Meteorological Station in Adrar, Algeria - 1 min, juillet 17 2014

Figure 5. Hourly evolution of the average wind speed [11].

IV. Description of Physical Model

The physical model used in this study is a parallelepiped-type habitable envelope composed of a single four-facade room, see Figure 6. The construction is located on a surface of $20m^2$. This room is built according to the following standards:

- The walls of the room are constructed of a light structure usually, 15 cm of block full of cement.

- The floor slab is placed on a flat earth. It is cast directly onto a 4cm layer of thermal insulation.

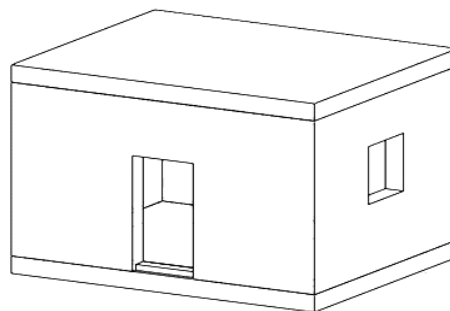- The roof consists of a slab of reinforced concrete.

Figure 6. Sketch of the piece studied.

V. Implementation of Model and Resolution

In this numerical study, we have opted for the nodal method use, which makes it possible to establish a thermal network equivalent to the modeling element. Conductive, convective and radiative processes are considered in global form (conservation of the heat flux). According to on the complexity of the network adopted, one can to incorporate all or part of the heat transfer phenomena, which allows predicting, with more precision, the thermal behavior of the studied part [13]. The phenomenological equation of heat relative to an infinitesimal volume makes it possible to write [14,15]:

$$\rho.Cp \frac{\partial T}{\partial t} d\tau + div(\phi).d\tau = P.d\tau \qquad (1)$$

With;

$\frac{\partial T}{\partial t}$: is the rate of variation of stored energy in $d\tau$;

$div(\phi)$: is the outgoing flow in $d\tau$;

$P.d\tau$: is the energy flow generated.

By integrating this expression on a volume Vi at temperature Ti, the energy balance is written [14-16,17]:

$$\rho.Cp_i.\frac{\partial T_i}{\partial t} = \varphi_{cond} + \varphi_{air} + \varphi_{conv} + \varphi_{radi} + P_i \qquad (2)$$

Or;

Cp_i : is the calorific capacity of the volume V_i.

P_i : is the source of flux dissipated in the volume V_i.

φ_{cond}, φ_{air}, φ_{conv} and φ_{radi}: are the flows exchanged between V_i and its environment by conduction, fluidic transport, convection and radiation.

The analog schematization in the Figure 7, we allow to propose an electric circuit amounting to the thermal system to be able to apply the law of Ohm [18,19,20].
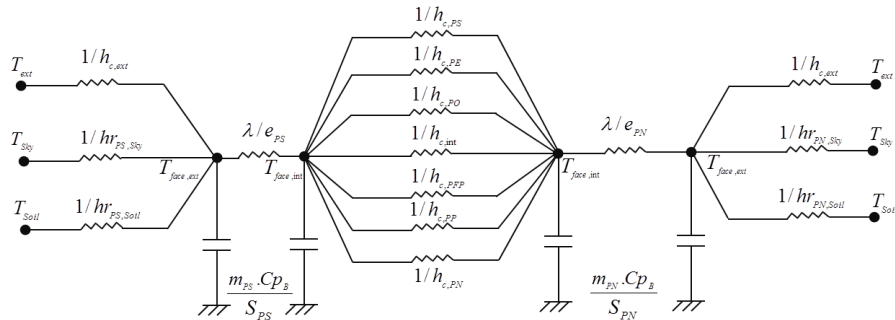

Figure. 7. Electrical map of the studied room.

The law enforcement of Ohm, in every knot of the studied room, gives the system of following equations:

- Thermal balances of external facades of the studied room

$$\begin{bmatrix} \dfrac{m_{PS}.Cp_b}{S_{PS}}.\dfrac{dT_{PSE}}{\Delta t} = h_{C,ext}.\Delta T + \dfrac{\lambda_b}{e}.\Delta T + hr_{VC-PSE}.\Delta T + hr_{SOL-PSE}.\Delta T + P_{absor} \\[2ex] \dfrac{m_{PS}.Cp_b}{S_{PN}}.\dfrac{T_{PNE}}{\Delta t} = h_{C,exct}.\Delta T + \dfrac{\lambda_b}{e}.\Delta T + hr_{VC-PNE}.\Delta T + hr_{SOL-PNE}.\Delta T + P_{absor} \\[2ex] \dfrac{m_{PO}.Cp_b}{S_{PO}}.\dfrac{dT_{POE}}{\Delta t} = h_{C,ext}.\Delta T + \dfrac{\lambda_b}{e}.\Delta T + hr_{VC-POE}.\Delta T + hr_{SOL-POE}.\Delta T + P_{absor} \\[2ex] \dfrac{m_{PFP}.Cp_b}{S_{PFP}}.\dfrac{dT_{PFPE}}{\Delta t} = h_{C,ext}.\Delta T + \dfrac{\lambda_b}{e}.\Delta T + hr_{VC-PFPE}.\Delta T + P_{absor} \\[2ex] \dfrac{m_{PE}.Cp_b}{S_{PE}}.\dfrac{dT_{PEE}}{\Delta t} = hr_{ext}.\Delta T + \dfrac{\lambda_b}{e}.\Delta T + hr_{VC-PEE}.\Delta T + hr_{SOL-PEE}.\Delta T + P_{absor} \end{bmatrix} \qquad (3)$$

- Thermal balance of interior facades of the studied room

$$
\begin{bmatrix}
\dfrac{m_{PS}.Cp_b}{S_{PS}}.\dfrac{dT_{PSI}}{\varDelta t} = h_{C,int}.\varDelta T + \dfrac{\lambda_b}{e}.\varDelta T + hr_{PSI-PNI}.\varDelta T + hr_{PSI-POI}.\varDelta T + \\[2pt]
hr_{PSI-PEI}.\varDelta T + hr_{PSI-PFPI}.\varDelta T + hr_{PSI-PIP}.\varDelta T \\[6pt]
\dfrac{m_{PN}.Cp_b}{S_{PN}}.\dfrac{dT_{PNI}}{\varDelta t} = h_{C,int}.\varDelta T + \dfrac{\lambda_b}{e}.\varDelta T + hr_{PNI-PSI}.\varDelta T + hr_{PNI-PEI}.\varDelta T + \\[2pt]
hr_{PNI-POI}.\varDelta T + hr_{PNI-PFPI}.\varDelta T + hr_{PNI-PIP}.\varDelta T \\[6pt]
\dfrac{m_{PO}.Cp_b}{S_{PO}}.\dfrac{dT_{POI}}{\varDelta t} = h_{C,int}.\varDelta T + \dfrac{\lambda_b}{e}.\varDelta T + hr_{POI-PSI}.\varDelta T + hr_{POI-PNI}.\varDelta T + \\[2pt]
hr_{POI-PEI}.\varDelta T + hr_{POI-PFPI}.\varDelta T + hr_{POI-PIP}.\varDelta T \\[6pt]
\dfrac{m_{PFP}.Cp_b}{S_{PFP}}.\dfrac{dT_{PFPI}}{\varDelta t} = h_{C,int}.\varDelta T + \dfrac{\lambda_b}{e}.\varDelta T + hr_{PFPI-PSI}.\varDelta T + hr_{PFPI-PNI}.\varDelta T + \\[2pt]
hr_{PFPI-POI}.\varDelta T + hr_{PFPI-PEI}.\varDelta T + hr_{PFPI-PIP}.\varDelta T \\[6pt]
\dfrac{m_{PE}.Cp_b}{S_{PE}}.\dfrac{dT_{PEI}}{\varDelta t} = h_{C,int}.\varDelta T + \dfrac{\lambda_b}{e}.\varDelta T + hr_{PEI-PSI}.\varDelta T + hr_{PEI-PNI}.\varDelta T + \\[2pt]
hr_{PEI-POI}.\varDelta T + hr_{PEI-PFPI}.\varDelta T + hr_{PEI-PIP}.\varDelta T \\[6pt]
m_a.Cp_a.\dfrac{dT_{int}}{\varDelta t} = h_{C1}.S_{PS}.\varDelta T + h_{C2}.S_{PN}.\varDelta T + h_{C3}.S_{PO}.\varDelta T + \\[2pt]
h_{C4}.S_{PE}.\varDelta T + h_{C5}.S_{PFP}.\varDelta T + h_{C6}.S_{PIP}.\varDelta T
\end{bmatrix}
\quad (4)
$$

The algebraic equations systems resulting from the discretization of transfer equations in both habitat environments (external and internal) are expressed in the form of matrices that can be written as:

$$ A \cdot x = B \qquad (5) $$

This equations system is solved by using the iterative numerical method of Gauss.

$$
\begin{bmatrix}
A_{11} & A_{12} & 0 & 0 & 0 & 0 & 0 & 0 & 0 & 0 & 0 \\
A_{21} & A_{22} & 0 & A_{24} & 0 & A_{26} & 0 & A_{28} & 0 & A_{210} & A_{211} \\
0 & 0 & A_{33} & A_{34} & 0 & 0 & 0 & 0 & 0 & 0 & 0 \\
0 & A_{42} & A_{43} & A_{44} & 0 & A_{46} & 0 & A_{48} & 0 & A_{410} & A_{411} \\
0 & 0 & 0 & 0 & A_{55} & A_{56} & 0 & 0 & 0 & 0 & 0 \\
0 & A_{62} & 0 & A_{64} & A_{65} & A_{66} & 0 & A_{68} & 0 & A_{610} & A_{611} \\
0 & 0 & 0 & 0 & 0 & 0 & A_{77} & A_{78} & 0 & 0 & 0 \\
0 & A_{82} & 0 & A_{84} & 0 & A_{86} & A_{87} & A_{88} & 0 & A_{810} & A_{811} \\
0 & 0 & 0 & 0 & 0 & 0 & 0 & 0 & A_{99} & A_{910} & 0 \\
0 & A_{102} & 0 & A_{104} & 0 & A_{106} & 0 & A_{108} & A_{109} & A_{1010} & A_{1011} \\
0 & A_{112} & 0 & A_{114} & 0 & A_{116} & 0 & A_{118} & 0 & A_{1110} & A_{1111}
\end{bmatrix}
\times
\begin{bmatrix}
T_{PSE}^{t+\varDelta t} \\
T_{PSI}^{t+\varDelta t} \\
T_{PNE}^{t+\varDelta t} \\
T_{PNI}^{t+\varDelta t} \\
T_{POE}^{t+\varDelta t} \\
T_{POI}^{t+\varDelta t} \\
T_{PFPE}^{t+\varDelta t} \\
T_{PFPI}^{t+\varDelta t} \\
T_{PEE}^{t+\varDelta t} \\
T_{PEI}^{t+\varDelta t} \\
T_{A2}^{t+\varDelta t}
\end{bmatrix}
=
\begin{bmatrix}
B_1 \\
B_2 \\
B_3 \\
B_4 \\
B_5 \\
B_6 \\
B_7 \\
B_8 \\
B_9 \\
B_{10} \\
B_{11}
\end{bmatrix}
\quad (6)
$$

Or:

$$ A_{11} = T_{PSE}^{t+\varDelta t} = \left(\frac{m_{PS}.Cp_{PS}}{S_{PS}}.\frac{1}{\varDelta t} + h_{C,ext} + \frac{\lambda_b}{e} + h_{rVC-PSE} + h_{rSOL-PSE} \right) \qquad (7) $$

$$A_{12} = T_{PSI}^{t+\Delta t} = \left(-\frac{\lambda_b}{e} \right) \tag{8}$$

$$B_1 = \left(\frac{m_{PS}.Cp_b}{S_{PS}}.\frac{T_{PSE}^t}{\Delta t} + h_{C,ext}.T_{ext}^t + h_{rVC-PSE}.T_{VC}^t + h_{rSOL-PSE}.T_{SOL}^t + P_{PS} \right) \tag{9}$$

$$A_{22} = T_{PSI}^{t+\Delta t} = \left(\frac{m_{PS}.Cp_b}{S_{PS}}.\frac{1}{\Delta t} + h_{C,int} + \frac{\lambda_b}{e} + h_{rPSI-PNI} + h_{rPSI-POI} + h_{rPSI-PEI} + h_{rPSI-PFPI} + h_{rPSI-PIP} \right) \tag{10}$$

The temperature of the thermal comfort (T_C) for a habitable one makes it possible to estimate the heating needs [21]. However, based on the bibliographic synthesis that was conducted in order to find a suitable model for the calculation of the comfort temperature, we opted for a relationship that was established between the comfort temperature (T_C), internal temperature (T_{int}) and mean radiant wall temperature (T_{PI}), as follows [22, 23]:

$$T_C = \frac{T_{int} + \sum_{n=1}^{n=6} T_{PI}}{2} \tag{11}$$

$$\sum_{n=1}^{n=6} T_{PI} = T_{PSI} + T_{PNI} + T_{PEI} + T_{POI} + T_{PFPI} + T_{PPI} \tag{12}$$

Taking into account the air as a transmission fluid between the ambiance and the room facades. Table 2 shows the physico-thermal properties of the air that were taken during the numerical simulation

Table 2. The Air Thermal Properties [23].

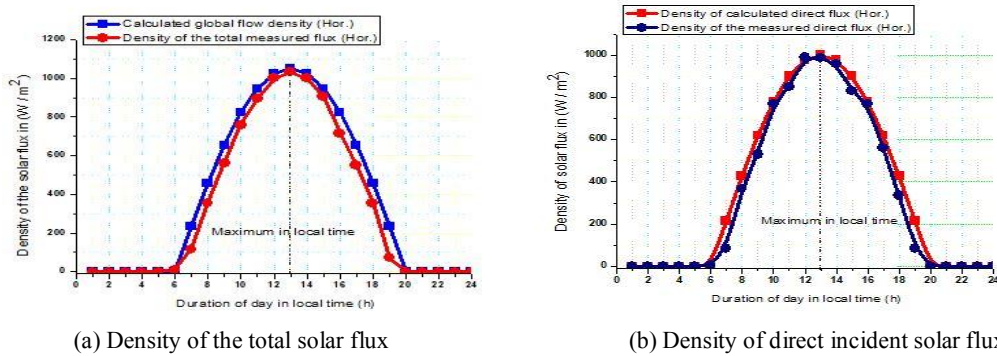|		
λ	Thermal conductivity in (W.m^{-1}.K^{-1})	0,0262
Cp	Specific heat in (J.Kg^{-1}.K^{-1})	1006
ρ	Density in (Kg.m^{-3})	1,177
μ	Dynamic viscosity in (Kg.m^{-1}.s^{-1})	$1,85.10^{-5}$
υ	Kinematic viscosity in (m^2.s^{-1})	$1,75.10^{-5}$
Pr	Number of Prandtl	0,708

VI. Results and discussion

VI.1. Validation of results

To test the validity of the models used to estimate the density of the solar flux, investigations were carried out on the global and direct solar flux density for a horizontal plane. The caliber models are used in the typical day of July 17th, 2014 in order to validate these estimating models by making a comparison with the measured data.

Figure 8 shows the calculated densities of the global (Fig.8a) and direct (Fig.8b) solar fluxes incident on a horizontal plane compared to those measured by the Adrar RERU'SM radiometric station. It can be observed that there is an acceptable agreement between the theoretical results and the experimental data, particularly in the middle of the day where the maximum relative difference does not exceed 1,8% for the case of the global solar flux and 1,5% for the case of the direct solar flux. Moreover, it can be also noted that the two types of

flux have the same variation trend.

| (a) Density of the total solar flux | (b) Density of direct incident solar flux |

Figure. 8. Calculated and measured solar flux densities for a horizontal surface during the 17th of July 2014 in the region of ADRAR.

VI.2. Internal evolution of temperature of the room

Figure 9 shows the hourly variation of the temperature of different internal facades of the room during the typical day. It can be seen that the thermal inertia of the concrete plays a very important role in the heat transfer at the walls. Indeed, the ceiling temperature (TPFP) is greater compared to the temperatures of the other internal faces of the South walls (TPSI), West (TPOI), North (TPNI) and East (TPEI).

This is due to the conjugation of two essential factors that led to this increase in temperature: in the first place, the walls thickness of the room which involves the elevation of the thermal inertia and secondly, the inclination angle of the roof facade which is equal to 0 °.
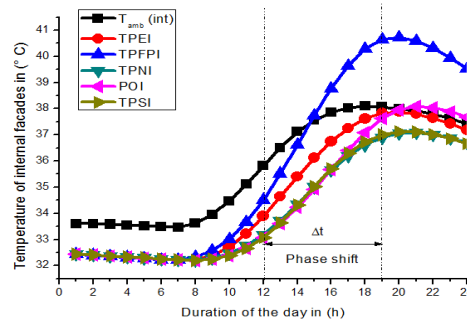

Figure. 9. Internal evolution of air temperature in the room, according to the local time.

VI.3. Internal evolution of temperature according to building materials

To use construction materials wisely, it is essential to know their thermal properties. The thermo-physical properties of the materials used in this study are shown in Table 3. The thermal capacity of a wall is especially useful if it is placed in the interior of the room and isolated from the external climatic conditions. To build in strong inertia, it is therefore to use heavy materials inside the room in order to store the solar heat and to attenuate the internal temperature variations [24]. Conversely, the temperature of a room with low inertia increases rapidly at the slightest ray of sun without the possibility of storing solar heat. Internal temperature differences will be significant and the risk of overheating will be high. Strong inertia is especially useful in case of permanent occupation. Low inertia can be interesting for habitable environments with intermittent use [24, 25].

Table 3. Thermophysical Properties of Building Materials [24, 25].

	Heavy concrete	Lightweight concrete	Concrete stone	Light wood	Heavy wood
Thermal conductivity λ (W.m^{-1}. K^{-1})	1,75	1,00	1,40	0,14	0,20
Density ρ (Kg.m^{-3})	2200	1500	1895	540	800
Specific heat Cp (J.kg^{-1}. K^{-1})	1000	1000	1000	2400	2700
Emissivity ε	0,54	0,54	0,54	0,86	0,86
Absorption coefficient α	0,6	0,6	0,6	0,07	0,07

Figure 10 illustrates the thermal capacity effect of solar energy storage in the room wall of for different building materials (light concrete, heavy concrete, stone concrete, light wood and heavy wood). It can be noted that for all habitable rooms built with high thermal capacity materials such as lightweight concrete (see Fig. 10(a)), heavy concrete (see Fig. 10(b)) and concrete stone (see Fig 10(c)), the temperature of its internal space is optimal in the month of July because of the thermal inertia of these materials. Indeed, it is well observed in figures (see Fig. 10(a), Fig.10(b) and Fig.10(c)) that the temperature of the internal ambiance varies between 37℃ and 38,5℃.

In addition, if the construction of habitable rooms is based on low heat capacity materials, the temperature of the internal space varies around 34℃ and 35℃ because of the thermal inertia of this building materials type (heavy wood (see Fig. 10(d)) and light wood (see Fig. 10(e)). Furthermore, it is noted that the temperature of the internal facades for building materials with high thermal capacity is very high compared to the internal facades of buildings with low heat capacity materials.
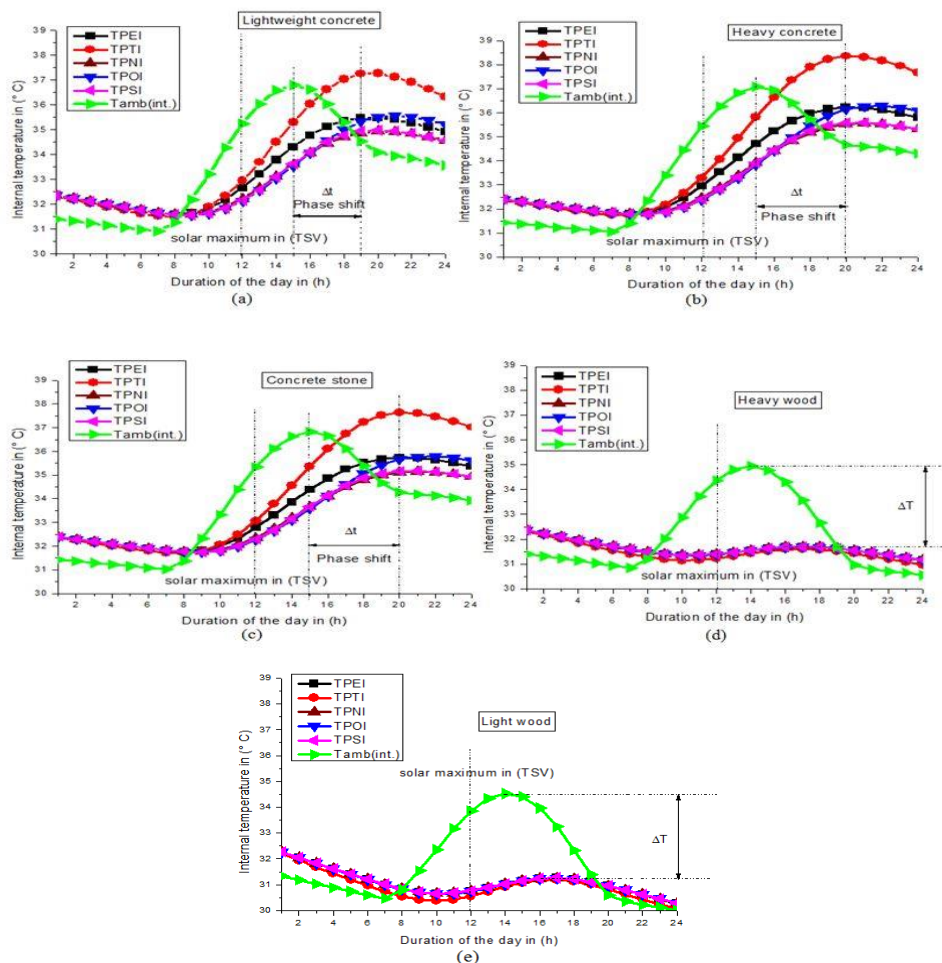

Figure. 10. Evolution of temperature of the room internal facades for different building materials.

VI.4. Evolution of the thermal comfort temperature

Figure 11 shows the hourly change in temperature of thermal comfort of different building materials as a function of local time. From this illustration, it can be seen that the choice of construction material has a significant influence on the hourly evolution of the thermal comfort temperature. Indeed, when one uses for example the concretes selected categories in this study as building material with these dry climatological conditions, and without control of thermal insulation, the comfort temperature will exceed the conventional norms. That is to say, undesirable overheating of the habitable environment with a temperature of 39°C at 15h00 in the afternoon as illustrated in Figure 11 for the three categories of concrete (heavy, light and stone).

On the other hand, the exploitation of other building materials such as the categories of wood (heavy and light) in this region with the same climatic conditions will help to get closer to the conventional values of the comfortable temperature in the environment. Habitable, since the maximum temperature obtained using the wood does not exceed 37°C (value obtained at 15h00 pm).
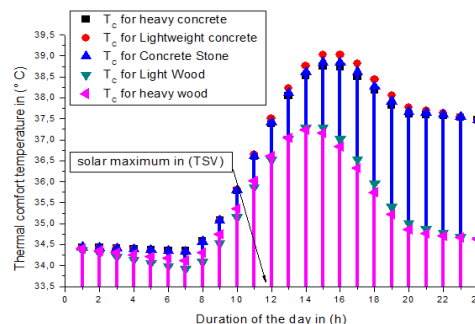

Fig. 11.   Evolution of the thermal comfort temperature in the room for different building materials in a typical day.

VI.5. Overlay on the psychrometric chart

Figure 10 shows the superimposition on the psychometric chart of temperature of thermal comfort within the room for different building materials in the typical day (July 17th, 2014). It can be seen that the thermal comfort temperature for concrete constructions (heavy, light and stone) is positioned in the zone MM' (zone of thermal inertia). While for both types of wood (heavy and light) is positioned in the same area as that of the concrete categories, except that the comfort temperature for a concrete construction varies between 38°C and 39°C and the temperature of a wood construction varies between 34°C and 36°C. Noting that these thermal comfort temperatures were calculated for the typical day of July 17th, 2014, which is the hottest day of the summer season in Adrar region.
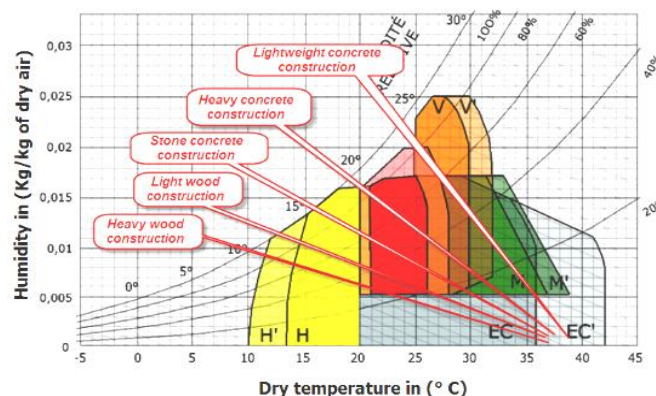

Figure. 12.   Super-positioning temperatures of thermal comfort of the room for different building materials during the typical day.

VII.   Conclusion

Thermal comfort is an essential element for the well-being of the occupant in his built environment. Taking it into account that the habitat implies their different aspects. However, after the numerical examination of the temperatures of different internal facades of the habitable room, the change effect of the building materials on the evolution of the internal temperature and the superposition of the thermal comfort temperatures on the psychometric chart, it has been found that:

- The use of bare concrete as a building material in the current architecture of Adrar region, involves undesirable overheating. In addition, the same effect has been noted for wood in this region, but with temperatures a little closer to conventional temperatures of thermal comfort.

- The severe climatic conditions of this region contribute in a direct way to the thermal discomfort.

On the basis of this study, it is recommended that before beginning the construction of a habitable envelope in this desert region, it is imperative to undertake an overall revision of conventional standards for thermal comfort, in particular the respect for bioclimatic concepts. On the other hand, we suggest:

- Ventilation and evaporative cooling during the summer season.

- Insulation and shading of the walls the most requested for excess solar radiation.

Acknowledgements

References

[1] A. Boursas, Etude de l'efficacité énergétique d'un bâtiment d'habitation à l'aide d'un logiciel de simulation, Magister Thesis, université of Constantine, Algeria, 2013.

[2] C. Batier, Confort thermique et énergie dans l'habitat social en milieu méditerranéen d'un modèle comportemental de l'occupant vers des stratégies architecturales, Ph.D. Thesis, université of Montpellier, la France, 2016.

[3] S. Alexis, Etudes de systèmes énergétiques et optimisation énergétique de bâtiments basse énergie, Master Thesis, université of Lorraine, la France, 2014.

[4] F. Errebai, L. Derradji, Y. Maoudj & M. Amara, Confort thermique d'un local d'habitation : Simulation thermoaéraulique pour différents systèmes de chauffage, Revue des Energies Renouvelables, Vol. 15 n°1, pp. 91 – 102, 2012.

[5] A. Sehli, A. Hasni & M.Tamali, the potential of earth-air heat exchangers for low energy cooling of buildings in South Algeria, Energy Procedia 18, pp. 496–506, 2012. DOI: 10.1016/j.egypro.2012.05.061.

[6] M. Benhammou, B. Draoui & M. Hamouda, Improvement of the summer cooling induced by an earth-to-air heat exchanger integrated in a residential building under hot and arid climate, Applied Energy 208, pp. 428–445, 2017. DOI: 10.1016/j.apenergy.2017.10.012.

[7] M. Benhammou, B. Draoui, M. Zerrouki & Y. Marif, Performance analysis of an earth-to-air heat exchanger assisted by a wind tower for passive cooling of buildings in arid and hot climate, Energy Conversion and Management 91, pp. 1–11, 2015. DOI:org/10.1016/j.enconman.2014.11.042

[8] H. Boutabba, M. Mili, S. Boutabba, L'architecture domestique en terre entre préservation et modernité: cas d'une ville oasienne d'Algérie (Aoulef) Domestic architecture in the ground between conservation and modernity: If an oasis city in Algeria, J. Mater. Environ., Sci. N°7 (10), pp. 3558-3570, 2016.

[9] F. Chellali, A. Khellaf, A. Belouchrani & A. Recioui, A contribution in the actualization of wind map of Algeria, Renewable and Sustainable Energy Reviews 15, pp. 993–1002, 2011. DOI:10.1016/j.rser.2010.11.025.

[10] A. Oudrane, Modélisation et caractérisation d'un système solaire destiné pour la production du chauffage des locaux, Magister Thesis, l'école polytechniques of Oran Maurice Audin, Algeria, 2011.

[11] Radiometric station, (EnerMENA), Technical Report, High Precision Meteorological Station of Research Unit for Renewable Energies in the Saharan Environment, in Adrar, Algeria, 2014.

[12] M. Peel, B. Finlayson & T. MacMahon, Updated world map of the Köppen-Geiger climate classification, Copernicus Publications pour European Geosciences Union, Göttingen, ISSN 1027-5606, In Hydrology and Earth System Sciences no 11, pp. 1633, 2007. DOI:org/10.5194/hess-11-1633-2007.

[13] M. Smaïl, Modélisation électromagnétique et thermique des moteurs à induction, en tenant compte des harmoniques d'espace, Ph.D. Thesis, université of lorraine, Nancy, la France, 2004.

[14] J. Lutun, Modélisation thermique des alternateurs automobiles, Ph.D. Thesis, université of Grenoble, la France, 2012.

[15] A. Jabbar, N. Khalifa & E. Abbas, A comparative performance study of some thermal storage materials used for solar space heating, Energy and Buildings 41, pp. 407–415, 2009. DOI: 10.1016/j.enbuild.2008.11.005.

[16] S. Bekkouche & T. Benouaz, Thermal resistances of local building materials and their effect upon the interior temperatures case of a building located in Ghardaïa region, Construction and Building Materials 52, pp. 59–70, 2014. DOI: 10.1016/j.conbuildmat.2013.10.052.

[17] A. Mezrhab & M. Bouzidi, Computation of thermal comfort inside a passenger car compartment, Applied Thermal Engineering 26, pp. 1697–1704, 2006. DOI:org/10.1016/j.applthermaleng.2005.11.008.

[18] F. Peuser, Remmers & Schnauss K., Installation solaires thermiques, conception et mise en œuvre, Edité par Systèmes Solaires, Solar Praxis et le Moniteur, 2005.

[19] M. Bekkouche, Modélisation du comportement thermique de quelques dispositifs solaires, Ph.D. Thesis, université of Tlemcen, Algeria, 2009.

[20] B. Amar, Contribution à l'étude de séchage solaire de produits agricoles locaux, Magister Thesis, université of Mentouri – Constantine, Algeria, 2010.

[21] S. Chandel & R. Aggarwal, Thermal Comfort Temperature Standards for Cold Regions, Ashdin Publishing Innovative Energy Policies, Vol. 2, Article ID E110201, pp. 5, 2012. DOI:10.4303/iep/E110201.

[22] M. Humphreys, Outdoor temperatures and comfort indoors, Batiment International, Building Research and Practice 6, pp. 92, 1978. DOI:org/10.1080/09613217808550656.

[23] F. Sam, Réhabilitation thermique d'un local dans une zone aride-Cas de Ghardaïa, Magister Thesis, université Mouloud Mammeri of Tizi Ouzou, Algeria, 2012.

[24] N. Tixier, Environnement thermique et maîtrise énergétique, ENSAG, Septembre 2012.

[25] L. Mavromatidis, M. EL Mankibi, Numerical estimation of time lags and decrement factors for wall complexes including multilayer thermal Insulation, in two different climatic zones, Applied Energy 92, pp. 480–491, 2012. DOI:org/10.1016/j.apenergy.2011.10.007.